Materials and Design 84 (2015) 300–312

Contents lists available at ScienceDirect

Materials and Design

journal homepage: www.elsevier.com/locate/jmad

A contact size-independent approach to the estimation of biaxial residual stresses by Knoop indentation

Felix Rickhey [a], Jin Haeng Lee [b], Hyungyil Lee [a,*]

[a] Sogang University, Department of Mechanical Engineering, Seoul 121-742, Republic of Korea
[b] Division for Research Reactor, Korea Atomic Energy Research Institute, Daejeon 305-353, Republic of Korea

ARTICLE INFO

Article history:
Received 21 March 2015
Received in revised form 1 June 2015
Accepted 20 June 2015
Available online 27 June 2015

Keywords:
Residual stress
Knoop indentation
Kick's law coefficient
Finite element analysis

ABSTRACT

The presence of residual stresses (RS) in a material causes a shift of the indentation load–displacement curve. The resulting change in the Kick's law coefficient *C* can hence be exploited to estimate these RS. By contrast with axisymmetric indenters, when employing the Knoop indenter with its large aspect-ratio, *C* is further sensitive to the indenter's orientation with respect to the principal RS directions. For a wide range of material properties, maximum and minimum *C* values are obtained by finite element analysis. It is observed that the RS ratio can be estimated directly from the *C* ratio, independent of magnitude and sign of RS. Further, the finding that *C* values for the non-equibiaxial RS case can be converted to equivalent *C* values for two equibiaxial RS cases, made for conical indentation (J.H. Lee et al., 2010, J Mater Res 25: 2212–2223), is shown to apply to Knoop indentation, too. The magnitude of RS can thus be determined from the equibiaxial RS case. The equibiaxial RS case is investigated in detail and mapping functions are established between *C* and the corresponding RS value. Finally the method is validated experimentally by comparison with Knoop indentation of bended cross-shaped steel specimens.

© 2015 Elsevier B.V. All rights reserved.

1. Introduction

Residual stresses (RS) are induced intentionally (*e.g.,* shot peening) or inevitably (*e.g.,* welding) and may affect fatigue life, corrosion or wear resistance significantly in a positive or negative way, depending on the application. In any way, estimating them is crucial when it comes to design. Several methods have been developed for measuring RS; destructive methods such as beam bending, hole-drilling [1], and non-destructive methods such as ultra-sonic methods, micromagnetic methods, neutron or X-ray diffraction [2]. Many of these methods are rather expensive or limited in their applicability. The highly versatile indentation test represents a simple non-destructive technique (though leaving a tiny impression), where specimen preparation is reduced to a minimum. For estimating RS from indentation, the differences in maximum indentation load, depth, hardness, elastic recovery or pile-up/sink-in behavior with RS (as compared with the virgin material) have been exploited.

By analyzing the influence of RS on the indentation load–displacement curves from finite element (FE) analysis and experiment, Tsui et al. [3] and Bolshakov et al. [4] showed that RS affect pile-up/sink-in behavior but not the contact area; the hardness decreases with increasing RS. To explain the fact that the RS effect is more pronounced for the tensile than for the compressive case, Sines and Carlson [5] provided a simple, yet illustrative mechanical model; while a uniaxial tensile RS increases the shear stress in the normal plane in which the RS lies and thus facilitates yielding, in the presence of uniaxial compressive RS, the maximum shear stress lies in a plane normal to the RS, which means that yielding is unaffected. As Tsui et al. [3] noted, this oversimplified model however loses its validity in later stages of indentation and when the equibiaxial RS case is approached.

Based on the argument that hardness (defined as the average contact pressure) is insensitive to equibiaxial RS, Suresh and Giannakopoulos [6] established a general methodology for predicting equibiaxial RS from sharp indentation and introduced a geometric factor that depends on the sign of RS. Giannakopoulos [7] later studied the more general case of biaxial RS and how they affect the indentation load–depth curve. Based on compressive RS evaluated by indentation tests and X-ray diffraction, Atar et al. [8] found that the shape factor in thin ceramic films is approximately unity. In a combined numerical and experimental study, Xu and Li [9] assessed the influence of biaxial RS on the unloading behavior and observed that there is a correlation between RS and hardness. However, they did not provide a model that relates RS to indentation parameters. Carlsson and Larsson [10,11] suggested replacing the yield stress by a combination of yield stress and RS to better agree with numerical and experimental results, yet missed out on presenting a model for general RS.

Using spherical indenters, Taljat and Pharr [12] proposed exploiting the influence of RS on the elastic–plastic transition. Swadener et al. [13] noted that spherical indenters may exhibit higher sensitivity of indentation properties to RS than Berkovich indenters. Their experimental

* Corresponding author at: Sogang University, Department of Mechanical Engineering, 35 Baekbom-ro, Seoul 121-742, Republic of Korea.
E-mail address: hylee@sogang.ac.kr (H. Lee).

http://dx.doi.org/10.1016/j.matdes.2015.06.119
0264-1275/© 2015 Elsevier B.V. All rights reserved.

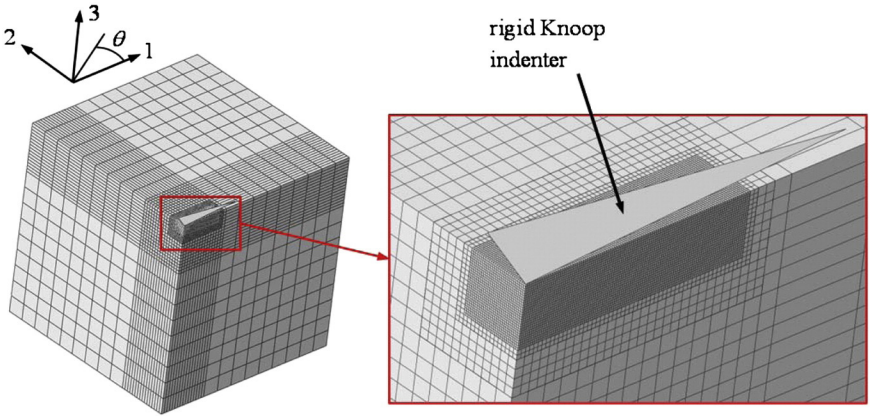

Fig. 1. Quarter FE model for Knoop indentation.

technique does not require imaging of the indent, but is restricted to equi-biaxial RS. Recently, Lu et al. [14] used the relative change in loading curvature to measure equibiaxial RS by conical indentation. Assuming elastic-perfectly plastic material behavior, Zhao et al. [15] and then Chen et al. [16] found a relationship between RS and material parameters by FE analysis and proposed a method that allows simultaneous determination of uniaxial or equibiaxial RS, yield strength and Young's modulus without requiring the contact area.

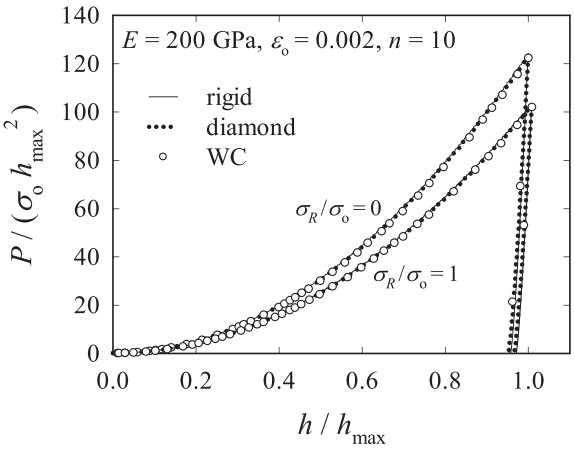

Fig. 2. Normalized P–h curves using rigid, diamond and WC indenters for σ_R/σ_o and 1.

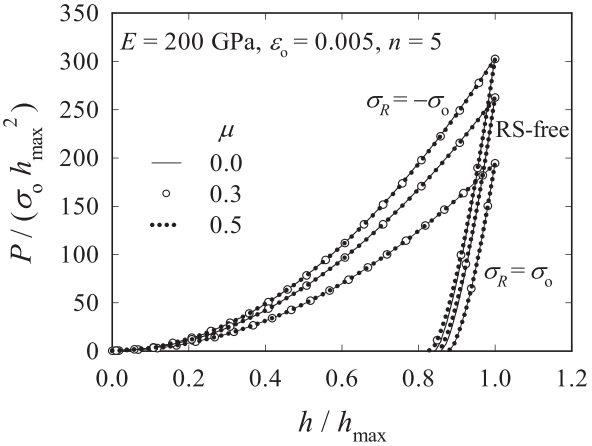

Fig. 3. Normalized P–h curves with $\mu = 0.0$, 0.3 and 0.5 (RS-free and $\sigma_R = \pm\sigma_o$).

Jang et al. [17] decomposed the RS into mean stress and deviatoric stress and concluded that among them only the deviatoric stress component in indentation direction affects the plastic deformation. Lee and Kwon [18] developed a stress-relaxation model and exploited the load difference between indentation on specimens with and without RS. The method relies on the impression size. However, differences in (the amount of) sink-in due to RS may make it difficult to obtain comparable contact areas, which may further deviate from the contact area inferred from contact stiffness. Based on this, Lee and Kwon [19] suggested a method for evaluating tensile and compressive non-equibiaxial RS from Vickers indentation by using the contact area (derived from contact stiffness) and the indentation load. The RS ratio can however not be obtained by this technique. Based on the directionality factor proposed by Lee and Kwon [18,19], Han et al. [20] and Choi et al. [21] noted the advantage of the Knoop indenter over other standardized indenters for non-equibiaxial RS evaluation, for the load–depth curve is now sensitive to the orientation of the indenter. An analytical model for tensile RS was provided that accounts for the different contributions of the non-equal RS to the corresponding load differences between stressed and unstressed material. Although the approach was in a good agreement with experiments on steel, the possible influence of material properties was not discussed. To obtain non-equibiaxial RS from the load–depth curve, Lee et al. [22] developed a conical indentation-based approach, but which requires pre-knowledge of the RS ratio. Groth and Mann [23] exploited the reduction of the short diagonal of the Knoop impression (due to elastic recovery

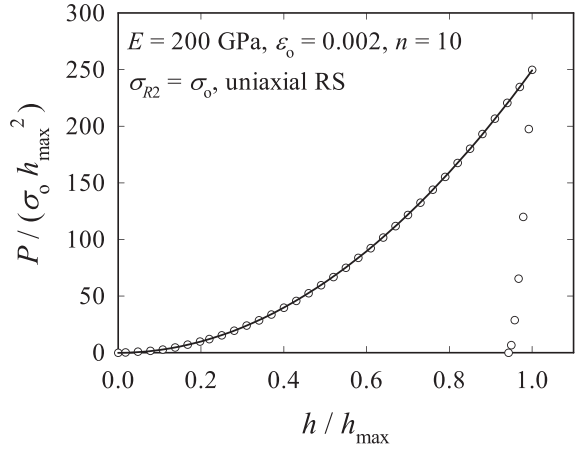

Fig. 4. Normalized P–h curves from FE analysis (circles) and based on regressed Kick's law coefficient (solid line).

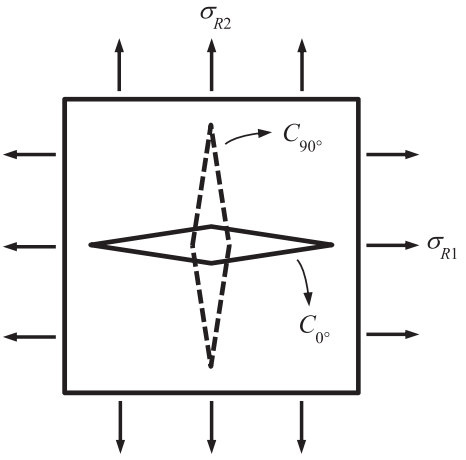

Fig. 5. Determination of $C_{0°}$ and $C_{90°}$ from P–h curves obtained by 2 Knoop indentations.

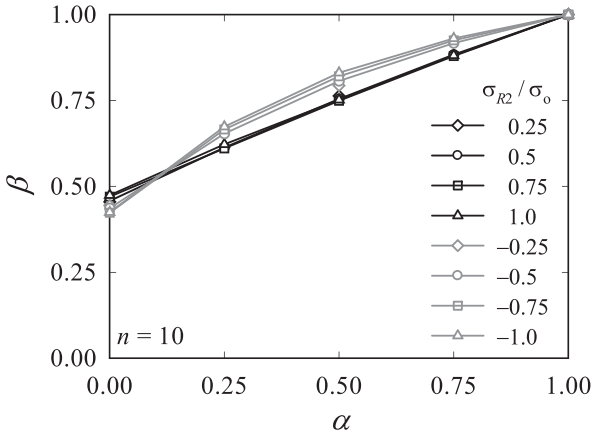

Fig. 7. β *vs.* α for diverse σ_{R2}/σ_o ($\varepsilon_o = 0.002$, $n = 10$): β is hardly affected by σ_{R2}/σ_o for a certain α.

during unloading) to estimate RS. Their approach is yet limited to metals which show sufficient recovery, *i.e.*, metals with low hardness-to-Young's modulus ratios.

In conclusion, a method for determining non-equibiaxial RS from indentation which takes into account the influence of material properties and which does not require the contact area (or contact stiffness) has not been developed yet. In this study, relying on finite element (FE) analysis we develop such an approach by investigating in detail the relation between Kick's law coefficient and elastic RS for a large range of materials characterized by their yield strain and hardening exponent. The sensitivity of Kick's law coefficient to the orientation of the Knoop indenter with respect to the RS is related to the RS ratio. Finally the method is validated by comparison with experiments on elastically bended cross-shaped specimens.

2. FE model for Knoop indentation and material model

All numerical analyses are performed using the commercial FE software Abaqus/Standard. The quarter FE model used for obtaining the Kick's law coefficient, shown in Fig. 1, is composed of 110,000 8-node brick elements (C3D8). The bottom surface nodes are fixed in 3-direction, whereas nodes on the outer surfaces are constrained in direction normal to the surface they lie in. Biaxial RS are imposed by Abaqus' initial condition option. The model size is chosen so that influences from the boundaries become negligible. Throughout this study, the maximum indentation depth is set to $h_{max} = 0.2$ mm, or 8 times the edge length e of an element of the innermost region. This mesh density is found to be sufficient because refining the mesh so that $h_{max} = 12$ e did not result in a change of the load-depth curve.

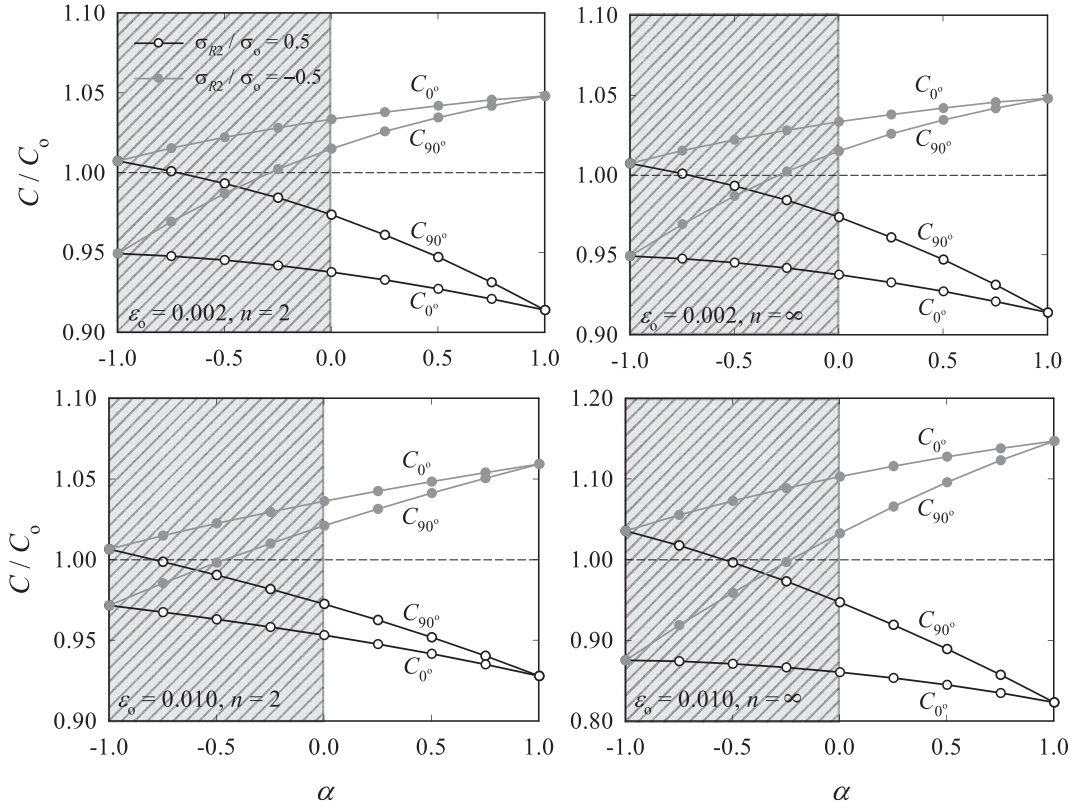

Fig. 6. Changes of $C_{0°}/C_o$ and $C_{90°}/C_o$ with α for $n = 2, \infty$ ($\varepsilon_o = 0.002, 0.010$); the case of negative α will not be treated in the remainder of this paper and is therefore hatched.

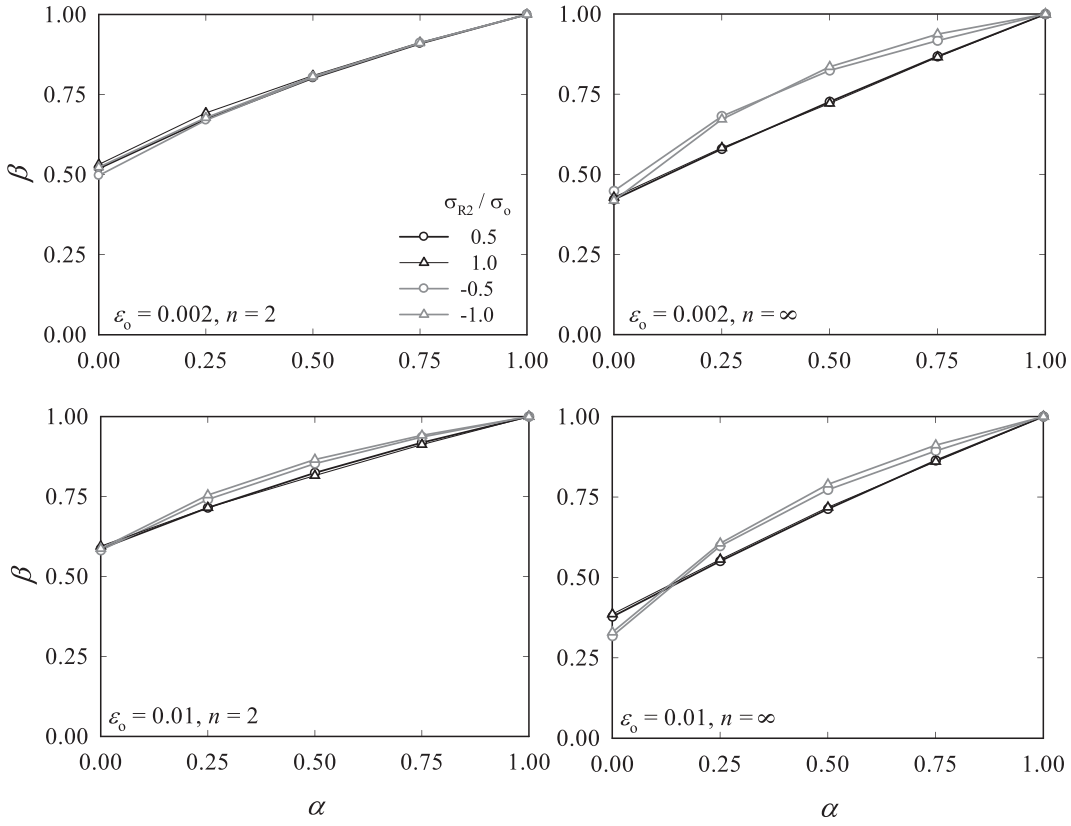

Fig. 8. β *vs.* α for $n = 2, \infty$ and $\varepsilon_o = 0.002, 0.01$.

The material is assumed to show Mises elastoplastic material behavior and permitted to undergo isotropic strain hardening. The stress–strain (σ–ε) relation is expressed by a piecewise power law (Hollomon-type stress–strain relation), which distinguishes between elastic and plastic regimes

$$\frac{\varepsilon}{\varepsilon_o} = \begin{cases} \dfrac{\sigma}{\sigma_o} & \text{for } \sigma \le \sigma_o \\ \left(\dfrac{\sigma}{\sigma_o}\right)^n & \text{for } \sigma > \sigma_o \quad ; \quad 1 < n < \infty \end{cases} . \tag{1}$$

Here n, ε and ε_o ($\equiv \sigma_o/E$) are strain hardening exponent, total strain and yield strain, respectively. σ_o and E denote initial yield stress and elastic modulus. Since E and σ_o of the indenter are usually much larger than those of the specimen, modeling is simplified by assuming a rigid indenter. This assumption can be justified by examining the indentation load–displacement (P–h) curves obtained with a rigid indenter and indenters made of common indenter materials, namely WC ($E = 537$ GPa, $\nu = 0.23$) and diamond ($E = 1140$ GPa, $\nu = 0.07$). The resulting load–displacement curves for the RS-free ($\sigma_R/\sigma_o = 0$) and the equibiaxial RS ($\sigma_R/\sigma_o = 1$) cases nearly coincide, as can be seen in Fig. 2 for a material with $E = 200$ GPa, $\nu = 0.3$, $\varepsilon_o = 0.002$ and $n = 10$; the maximum deviation of 1% in the maximum indentation load may be neglected in light of the reduced computational costs. Friction between the Knoop indenter and the material surface is considered with Coulomb friction coefficient $\mu = 0.3$. Friction has

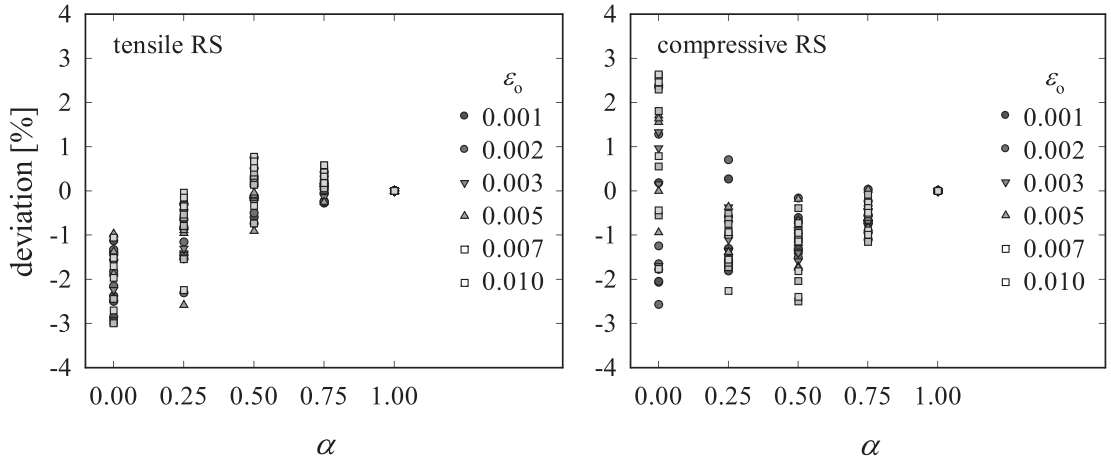

Fig. 9. Deviation $(\beta_{1.0} - \beta_{0.5}) / (\beta_{1.0} + \beta_{0.5})$ from the assumption that β is not influenced by the magnitude σ_{R2}/σ_o for a given α, for tensile and compressive RS.

Table 1
Material properties from spherical indentation test.

Specimen	Number	Maximum load [N]	E [GPa]	σ_o [MPa]	n
SS400 specimen	1	861	210	244	6.57
	2	863	199	231	5.98
	3	862	181	271	7.43
	4	859	215	220	5.86
	5	855	211	194	5.05
	Avg.	860	207	232	6.14
SM45C specimen	1	1194	199	298	4.87
	2	1196	190	309	5.01
	3	1200	184	359	5.93
	4	1194	190	315	5.09
	5	1200	204	353	6.02
	Avg.	1197	193	326	5.34

Table 2
Applied stresses *via* strain gauge and RS from indentation test.

Material	Strain gauge [MPa]		Indentation [MPa]		Error in σ_{R1} [%]	Error in σ_{R2} [%]	Error in α [%]
	σ_{R1}	σ_{R2}	σ_{R1}	σ_{R2}			
SS400	136	103	130	105	4.4	−1.9	−6.6
	103	87	101	89	1.5	−2.3	−4.3
	103	0	118	12	−14.6	–	–
SM45C	136	136	141	142	−3.7	−4.4	−0.7
			150	149	−10.3	−9.6	0.7
	136	119	145	129	−6.6	−8.4	−1.7
			122	105	10.3	11.8	1.6
	127	97	126	104	0.8	−7.2	−8.1
	97	78	82	69	15.5	11.5	−4.6
	97	0	106	11	−9.3	–	–
	84	62	97	70	−15.5	−12.9	2.2
			87	64	−3.6	−3.2	0.3
			83	61	2.1	2.1	0.4
	62	50	56	45	12.4	8.8	0.4
			55	44	19.7	11.8	0.8

however a negligible effect on the load–depth curves, regardless of magnitude and sign of RS and material properties (Fig. 3); the error in the maximum load lies well below 1%. Fig. 3 indicates that apart from the load the final depth is affected by the RS; compressive RS support the recovery of the impression while tensile RS lead to an increase in the final depth. The relative change is however lower than the relative change in maximum loads; further, accurate measurement of the impression size is rather problematic.

The load–displacement (P–h) curve for sharp indentation follows Kick's law

$$P = Ch^2. \tag{2}$$

A change in the maximum indentation load, ΔP, due to the presence of RS results in a proportional change of Kick's law coefficient, $\Delta C = \Delta P/h^2$. The Kick's law coefficient C is used as indentation variable because the effect of unavoidable tip rounding on C can be readily accounted for, as outlined in Lee et al. [24]. C depends on material properties; yet, if C is normalized by E, the ratio C/E can be taken as a representative value for materials which have equal ε_o and n (*i.e.*, every combination of ε_o and n yields a unique C value). Throughout this study, we assume $E = 200$ GPa; however, our suggested method will be applicable to other values of E because the key parameter is ε_o, not the absolute values of E or σ_o [25]. While Poisson's ratio is set to $\nu = 0.3$, yield strain and hardening exponent are varied within the range $\varepsilon_o = [0.001, 0.01]$ and $n = [2, \infty]$, so that the range of common metals is covered.

The Kick's law coefficient is obtained by fitting load–depth data to Eq. (2). Since load–displacement data at very low indentation depths may be inaccurate in real indentation due to tip rounding, only data between 0.5 h_{max} and h_{max} are considered. The FE load–depth curve is in an excellent agreement with the load–depth curve based on the Kick's law coefficient from regression, as we can see in Fig. 4 for $\sigma_{R1} = 0$ and $\sigma_{R2} = \sigma_o$. By contrast with conical indentation, Knoop indentations with the major indenter axis aligned with (1) the minor absolute principal RS σ_{R1} (orientation angle $\theta = 0°$) and (2) the major absolute principal RS σ_{R2} ($|\sigma_{R2}| > |\sigma_{R1}|$) ($\theta = 90°$) deliver two non-equal C values, denoted by the extrema $C_{0°}$ and $C_{90°}$ (Fig. 5). Due to the large aspect ratio of the Knoop indenter, C is quite sensitive to θ, thereby making the indenter a predestined tool for evaluating arbitrary RS. Obviously, the sensitivity of the difference in C could be maximized by increasing the aspect ratio, but this would result in a very sharp, wedge-like indenter. Due to its wide availability, the standard Knoop indenter is the preferred tool here.

3. FE results and observations

We denote the Kick's law coefficient of the virgin (*i.e.*, RS-free) material by C_o and the RS ratio by $\alpha \equiv \sigma_{R1}/\sigma_{R2}$ ($-1 \le \alpha \le 1$). Values of $C_{0°}/C_o$ and $C_{90°}/C_o$ are plotted against α for $\sigma_{R2}/\sigma_o = \pm 0.5$ (Fig. 6). The case of negative α (*i.e.*, mixed positive and negative RS) will not be treated any further after this paragraph; nevertheless we add the case of mixed RS to Fig. 6 because we think that this may be of interest for future studies. Fig. 6 reveals that both σ_{R1} and σ_{R2} contribute to the difference in C between RS-free and stressed specimens, although the RS component normal to the median plane through the major indenter diagonal causes a higher change. In particular for compressive RS, where the RS effect is less pronounced, the difference between $C_{0°}$ and $C_{90°}$ can be rather small. However noting that load–displacement data can be obtained very accurately and reliably from indentation tests, even relatively small differences are sufficient. Further, as we will see later, we are interested in the differences $(C_o - C_{0°})/C_o$ and $(C_o - C_{90°})/C_o$. For non-negative α, the following qualitative statements can be deduced from Fig. 6; firstly, if both $C_{0°}$ and $C_{90°}$ are below C_o, RS must be tensile, *i.e.*, $\sigma_{R1}, \sigma_{R2} > 0$, whereas if they are above C_o, RS must be compressive, *i.e.*, $\sigma_{R1}, \sigma_{R2} < 0$. This is because tensile RS make it easier for the indenter to penetrate the material since they support the material flow away from the center, whereas compressive RS work against the indentation. Consequently, indentation on a material under compressive RS requires a higher load and thus yields a higher C value. Provided C_o is known, we can thus by only one indentation ascertain whether RS are tensile or compressive, which means that the two cases can be treated independently. Secondly, if $C_{0°} < C_{90°}$ then

Table 3
Coefficients for Eq. (7).

		$i = 1$			$i = 2$		
		$j = 0$	$j = 1$	$j = 2$	$j = 0$	$j = 1$	$j = 2$
f_α^+	$k = 0$	1.359E+0	−1.471E+0	−2.904E+0	3.738E−1	1.857E+0	1.146E+0
	$k = 1$	−7.412E+1	3.646E+2	−6.716E+2	−9.962E−1	−4.591E+2	8.087E+2
	$k = 2$	3.516E+3	5.833E+2	−8.384E+3	1.045E+3	1.491E+4	−1.173E+4
f_α^-	$k = 0$	−2.981E+0	9.885E+0	−1.064E+1	3.355E+0	−6.699E+0	7.814E+0
	$k = 1$	5.300E+2	−9.606E+2	1.366E+2	−3.891E+2	4.614E+2	1.602E+2
	$k = 2$	−2.580E+4	2.453E+4	−7.428E+4	1.837E+4	5.016E+3	2.426E+4

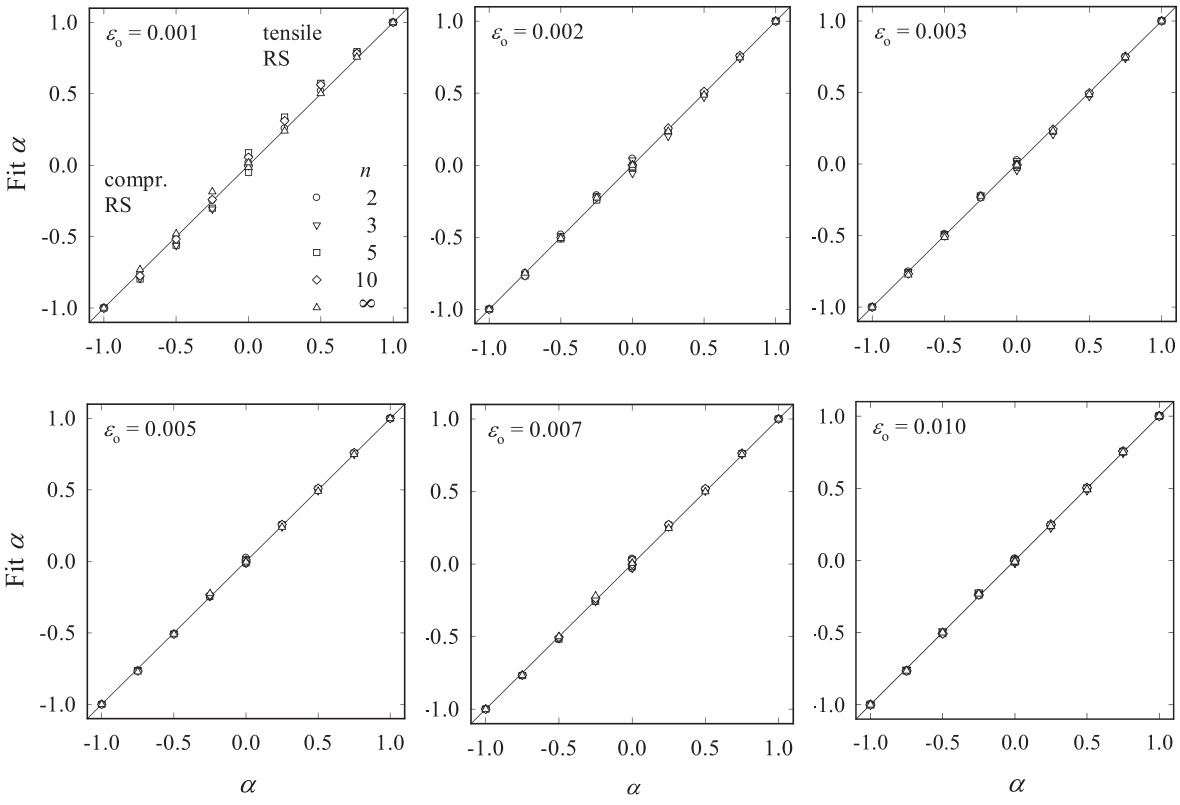

Fig. 10. Deviation of α calculated by Eq. (7), "Fit α", from FE input values.

$\sigma_{R1} < \sigma_{R2}$. Thirdly, the higher the gap between mean average $(C_{0^\circ} + C_{90^\circ})$ / 2 and C_o, the higher is the absolute sum of RS, $|\sigma_{R1} + \sigma_{R2}|$.

Generally, although this cannot be seen directly from Fig. 6, where C – either C_{0° or C_{90° – is normalized by C_o, a decrease in n (pronounced hardening) or an increase in ε_o lead to an increase in C. Raising the magnitude of compressive RS results in an increase in C, whereas raising the magnitude of tensile RS leads to a decrease in C. For the range of materials chosen in this study, the maximum C is consequently obtained for the case "maximum α (=1, equibiaxial RS), minimum σ_{R2}/σ_o (=−1), minimum n (=2) and maximum ε_o (=0.01)". However, the *ratio* C/C_o becomes maximum for $\alpha = 1$, $n = \infty$ and $\varepsilon_o = 0.01$.

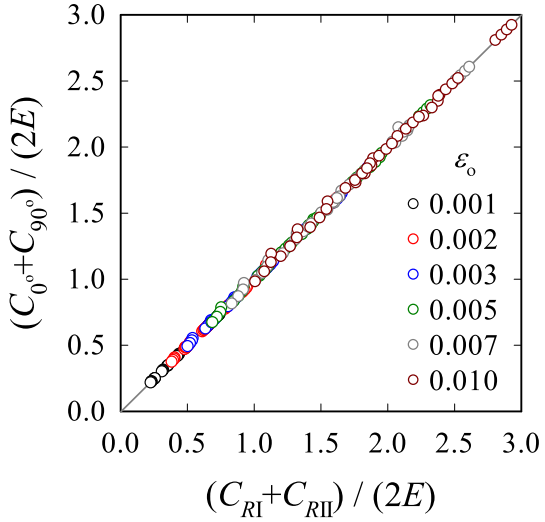

Fig. 11. Deviation of FE results from Eq. (8).

Applying the Buckingham Pi theorem, the Kick's law coefficient for the RS-free case can be expressed in terms of material properties as

$$\frac{C_o}{E} = \Pi_o(\nu, \varepsilon_o, n). \tag{3}$$

As compared with the RS-free case, additional terms enter the expressions for C_{0° and C_{90°. We may write

$$\begin{aligned} \frac{C_{0^\circ}}{\sigma_o} &= g_{0^\circ}\left(\nu, \varepsilon_o, n, \alpha, \frac{\sigma_{R2}}{\sigma_o}\right) \\ \frac{C_{90^\circ}}{\sigma_o} &= g_{90^\circ}\left(\nu, \varepsilon_o, n, \alpha, \frac{\sigma_{R2}}{\sigma_o}\right). \end{aligned} \tag{4}$$

Based on the statements made in Section 3, we define two dimensionless variables

$$\begin{aligned} \beta &\equiv \frac{C_o - C_{90^\circ}}{C_o - C_{0^\circ}} \\ \chi &\equiv \frac{1}{2}\left(\frac{C_o - C_{0^\circ}}{C_o} + \frac{C_o - C_{90^\circ}}{C_o}\right) = \frac{C_o - (C_{0^\circ} + C_{90^\circ})/2}{C_o} \end{aligned} \tag{5}$$

where β is to represent the ratio $\alpha = \sigma_{R1}/\sigma_{R2}$ and χ is to represent the normalized sum of RS, *i.e.*, $(\sigma_{R1} + \sigma_{R2})/\sigma_o$. The variables are chosen so that both β and χ rise monotonically with α and $(\sigma_{R1} + \sigma_{R2})/\sigma_o$, respectively. Further, $0 < \beta \le 1$, and $\chi > 0$ for tensile RS and $\chi < 0$ for compressive RS. Note that for very low RS, β becomes quite sensitive to inaccuracies in C values because numerator and denominator approach zero. Thus one must be cautious in using Eq. (5) when all three C values are very close to each other. We will get back to this issue at the end of Section 4.4.

β values are plotted against α $(0 \le \alpha \le 1)$ for $\sigma_{R2}/\sigma_o = \pm 0.25, \pm 0.5, \pm 0.75$ and ± 1.0 in Fig. 7 ($\varepsilon_o = 0.002$, $n = 10$). The curves for tensile RS nearly coincide as well as the curves for compressive RS, which means that β is hardly affected by σ_{R2}/σ_o for a given α. As can be seen in

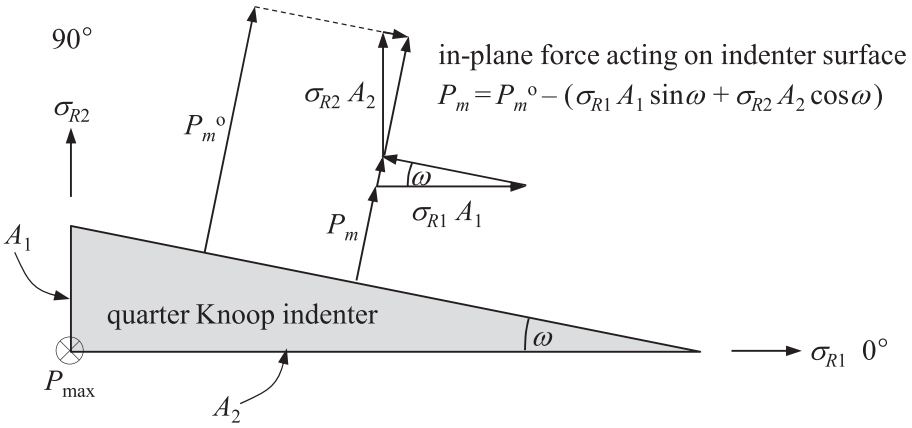

Fig. 12. Analytical model: displayed is the configuration for obtaining $C_{0°}$; for obtaining $C_{90°}$ the indenter is rotated by 90° about the loading axis [top view] (all forces are in-plane forces).

Fig. 8 for combinations of minimum and maximum ε_o and n values, this holds approximately for other materials, too; the deviation of β for $\sigma_{R2}/\sigma_o = 1.0$ ($\beta_{1.0}$) from the mean average of β values obtained with $\sigma_{R2}/\sigma_o = 0.5$ ($\beta_{0.5}$) and 1, *i.e.*, $(\beta_{1.0} - \beta_{0.5}) / (\beta_{1.0} + \beta_{0.5})$, is below 3% for the whole range of materials (Fig. 9). The fact that the curves for higher σ_{R2}/σ_o lie almost always above those with lower σ_{R2}/σ_o (Fig. 7, Fig. 8), in other words, that the deviation in Fig. 9 is mainly negative, and the fact that the deviation increases with decreasing α indicate that the assumption that β be not affected by σ_{R2}/σ_o for a given α may not be strictly correct, at least not for tensile RS; yet the deviation over the whole range of elastic RS is very small in light of the simplification it entails. Further, although for high-hardening materials (low n) the curves for tensile and compressive RS nearly coincide, Fig. 7 and Fig. 8 support the proposition that tensile and compressive RS cases are fundamentally different — as the theoretical model by Suresh and Giannakopoulos [6] and the discussions by Carlsson and Larsson [10,11], Huber and Heerens [26], Larsson [27] revealed. The tensile RS curves are nearly straight regardless of ε_o and n, while the ones for compressive RS change from approximately straight to curved with increasing ε_o and n. The observation made for tensile RS is in agreement with Han et al. [20], who conducted Knoop indentation tests on API X65 steel specimens. The load difference ratio (equivalent to β) for $\alpha = 0$ (tensile RS), which they reported to be 0.34 for API X65, however is material-dependent.

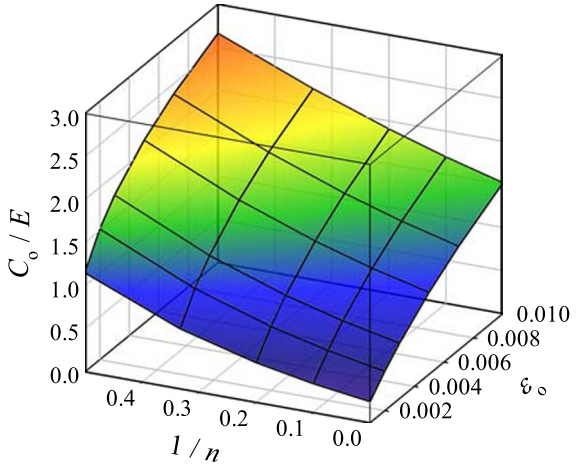

Fig. 13. FE results for C_o/E assuming diverse combinations of ε_o and n.

4. Determination of residual stresses

4.1. Residual stress ratio

Assuming that the small influence of σ_{R2}/σ_o on β for a certain α can be disregarded for $\alpha \geq 0$, we can directly determine α from β for a certain combination of ε_o and n, independent of σ_{R1}/σ_o and σ_{R2}/σ_o, which facilitates the establishment of mapping functions significantly. Neglecting further the effect of Poisson's ratio, which has been set to $\nu = 0.3$, and using dimensional analysis, we can write

$$\begin{aligned} &\alpha = f_\alpha^+(\beta, \varepsilon_o, n) \quad \text{for } C_{0°}, C_{90°} < C_o \quad \text{(tensile RS)} \\ &\alpha = f_\alpha^-(\beta, \varepsilon_o, n) \quad \text{for } C_{0°}, C_{90°} > C_o \quad \text{(compressive RS)}. \end{aligned} \tag{6}$$

For the fitting functions $f_\alpha{}^+$ and $f_\alpha{}^-$, a 2nd degree polynomial function of the form

$$\begin{aligned} &\alpha = 1 + A_i(\varepsilon_o, n)\ \left(1 - \beta^i\right) \\ &A_i(\varepsilon_o, n) = B_{ij}(\varepsilon_o)\ n^{-j} \\ &B_{ij}(\varepsilon_o) = C_{ijk}{\varepsilon_o}^k \quad ; \quad i = 1,\ 2 \quad ; \quad j,\ k = 0,\ 1,\ 2 \end{aligned} \tag{7}$$

gives a sufficiently accurate fit to the FE data. Note that the transition between f_i^- and f_i^+ is continuous, but not the transition between their derivatives. Coefficients for $f_\alpha{}^+$ and $f_\alpha{}^-$ are provided in Table 3. Only for the smallest yield strain, $\varepsilon_o = 0.001$, the deviation is somewhat higher (Fig. 10). However, the sensitivity of C to RS is rather low here (especially in combination with a high n), making the approach less appropriate for these materials.

Lee et al. [22] found for conical indentation that the maximum load (or C) for indentation on a specimen with σ_{R1} and σ_{R2} is equal to the mean average of the maximum loads (or C) from two indentations (same depth) on specimens with equibiaxial RS $\sigma_{RI} = \sigma_{R1}$ and $\sigma_{RII} = \sigma_{R2}$. Assuming that this holds also for Knoop indentation, we can write in terms of Kick's law coefficients in a similar fashion

$$C_{0°} + C_{90°} = C_{RI} + C_{RII} \quad \leftrightarrow \quad \chi = \frac{C_o - (C_{0°} + C_{90°})/2}{C_o} = \frac{C_o - (C_{RI} + C_{RII})/2}{C_o} \tag{8}$$

Table 4
Coefficients for Eq. (14).

b_{ij}	$j = 0$	$j = 1$	$j = 2$	$j = 3$
$i = 0$	0.000E+0	2.636E+2	−1.768E+4	6.503E+5
$i = 1$	1.853E−1	4.486E+2	−5.143E+4	2.181E+6
$i = 2$	2.552E+0	−6.464E+1	−1.881E+4	1.139E+6

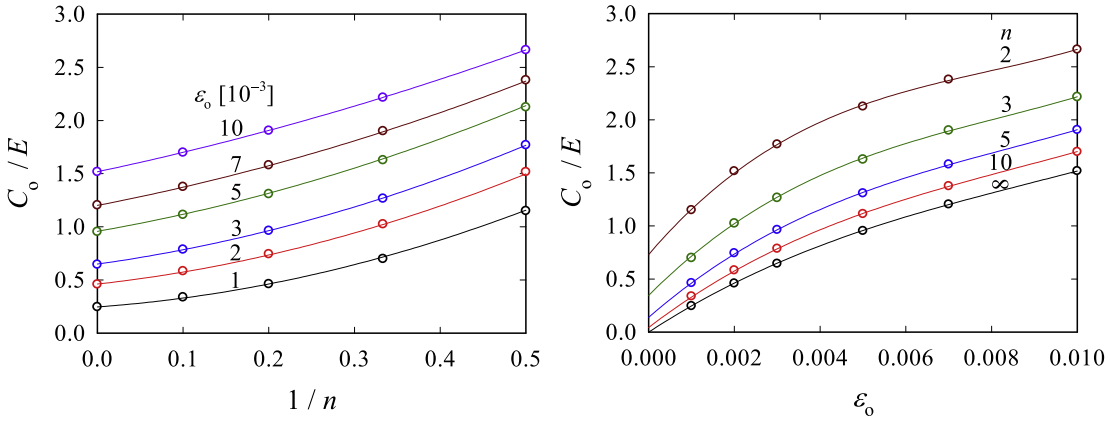

Fig. 14. Change of C_o/E with ε_o and n; solid lines are the corresponding fitting curves (Eq. (14)).

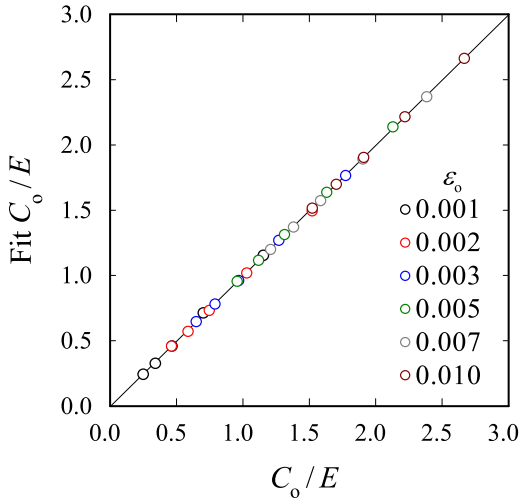

Fig. 15. Comparison of C_o/E obtained by Eq. (14), "FitCo/E", with FE results for 30 materials.

where C_{RI} and C_{RII} denote the Kick's law coefficients obtained from indentations on a specimen subject to equibiaxial RS σ_{RI} and on a specimen subject to equibiaxial RS σ_{RII}. Comparison of $(C_{0^\circ} + C_{90^\circ}) / (2E)$ with corresponding $(C_{RI} + C_{RII}) / (2E)$ values for $\alpha = 0$, 0.25, 0.5 and 0.75 and $\sigma_{R2}/\sigma_o = \pm 1$ (8 combinations × 30 materials = 240 data) shows that Eq. (8) indeed holds for Knoop indentation (Fig. 11). The small error (maximum error <2%, average error = 0.5%) is not systematic and therefore probably due to numerical inaccuracies. This means that RS can be obtained by finding virtual Kick's law coefficients C_{R1} and C_{R2} that yield the same α. This conversion is very convenient because the function for the equibiaxial RS case requires one fewer variable than Eq. (4), for α is known to be 1.

As the concept applies to conical and Knoop indenters, we may expect it to be applicable to any sharp indenter. A simple analytical model can be established that corroborates the numerical finding (Fig. 12). All forces in Fig. 12 act in-plane and all indentations are performed to equal h_{max}. As we have concluded from the discussion regarding Fig. 6, both RS contribute to the change in C_{0° and C_{90° with respect to C_o. We expect, in light of self-similarity, that the in-plane force P_m, as shown in Fig. 12, scales with the applied load, P_{max}, *i.e.*,

$$P_m = k\ P_{max} \tag{9}$$

where the proportionality factor k depends on the indenter shape – represented through the indenter angle(s) φ; for the Knoop indenter $\varphi_1 = 86.25^\circ$ and $\varphi_2 = 65^\circ$ – only. Similarly, the difference in P_m between the RS-free and the RS cases scales with the corresponding indentation load difference, *i.e.*, $\Delta P_m = k\,\Delta P_{max}$. Further, the change in pile-up/sink-in behavior due to RS is neglected so that $A_1/A_2 = \text{const.}$, where A_1 and A_2 are the normal cross-sections through the minor and major indenter diagonals, respectively (Fig. 12).

For the *general biaxial* case, the absolute differences in loads necessary for indentations to h_{max} (with respect to the RS-free case, denoted by the superscript 'o') can be written as

$$\begin{aligned} \Delta P_m^{0^\circ} &= P_m^{0^\circ} - P_m^{o} = \sigma_{R1} A_1 \sin\omega + \sigma_{R2} A_2 \cos\omega \quad \rightarrow \quad \Delta P_{max}^{0^\circ} = \kappa_1 \sigma_{R1} + \kappa_2 \sigma_{R2} \\ \Delta P_m^{90^\circ} &= P_m^{90^\circ} - P_m^{o} = \sigma_{R2} A_1 \sin\omega + \sigma_{R1} A_2 \cos\omega \quad \rightarrow \quad \Delta P_{max}^{90^\circ} = \kappa_1 \sigma_{R2} + \kappa_2 \sigma_{R1} \end{aligned} \tag{10}$$

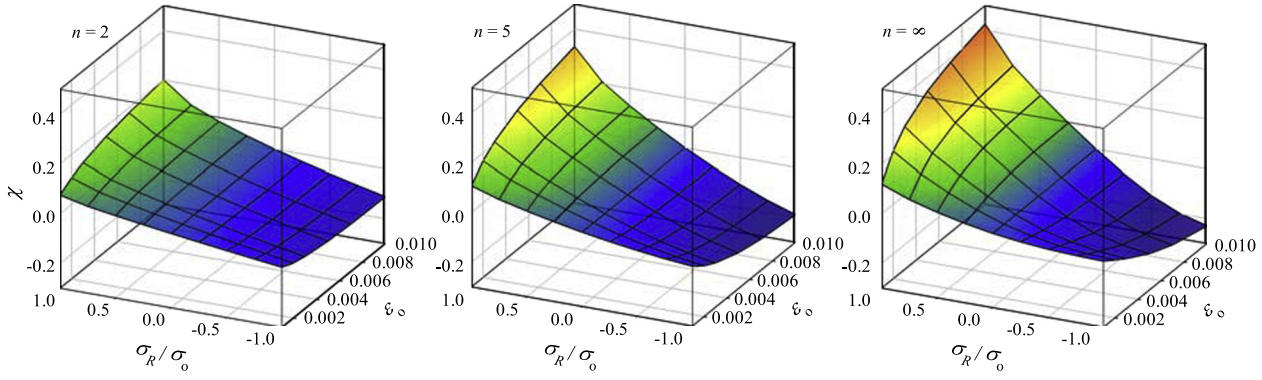

Fig. 16. Change of χ with ε_o and σ_R/σ_o for $n = 2, 5, \infty$.

Table 5
Coefficients for Eq. (15).

		$i=1$			$i=2$		
		$j=0$	$j=1$	$j=2$	$j=0$	$j=1$	$j=2$
f_R^+	$k=0$	2.242E+0	7.442E+0	2.926E+0	−1.622E+0	−9.724E+0	−2.169E+1
	$k=1$	6.780E−3	−8.627E−3	4.075E−2	4.427E−3	3.384E−3	−1.122E−1
	$k=2$	3.517E−6	−5.769E−6	−1.149E−5	−3.767E−5	7.578E−5	−6.798E−5
f_R^-	$k=0$	1.266E+0	8.045E+0	6.129E+0	6.927E+0	−4.828E+1	3.800E+1
	$k=1$	4.478E−3	−4.014E−4	2.851E−2	−1.443E−1	5.659E−1	−5.533E−1
	$k=2$	7.755E−6	−4.029E−5	4.185E−5	−1.356E−4	3.637E−4	−2.350E−4

$\kappa_1 = A_1 \sin\omega/k$ and $\kappa_2 = A_2 \cos\omega/k$ depend on the indenter shape only ($\tan\omega = \tan\varphi_2/\tan\varphi_1$). For the two *equi-biaxial* cases (I: $\sigma_{RI} = \sigma_{R1}$; II: $\sigma_{RII} = \sigma_{R2}$), we get

$$\begin{aligned} \Delta P_m^{I} &= \sigma_{RI}(A_1 \sin\omega + A_2 \cos\omega) \quad \rightarrow \quad \Delta P_{max}^{I} = (\kappa_1 + \kappa_2)\sigma_{RI} \\ \Delta P_m^{II} &= \sigma_{RII}(A_1 \sin\omega + A_2 \cos\omega) \quad \rightarrow \quad \Delta P_{max}^{II} = (\kappa_1 + \kappa_2)\sigma_{RII} \end{aligned} \tag{11}$$

Summing up the cases {0°, 90°} and {I, II} and comparing them leads to

$$\left.\begin{aligned} &\Delta P_{max}^{0^\circ} + \Delta P_{max}^{90^\circ} = \kappa_1(\sigma_{R1} + \sigma_{R2}) + \kappa_2(\sigma_{R1} + \sigma_{R2}) \\ &\Delta P_{max}^{I} + \Delta P_{max}^{II} = (\kappa_1 + \kappa_2)\sigma_{RI} + (\kappa_1 + \kappa_2)\sigma_{RII} \end{aligned}\right\} \rightarrow \Delta P_{max}^{0^\circ} + \Delta P_{max}^{90^\circ} = \Delta P_{max}^{I} + \Delta P_{max}^{II} \tag{12}$$

or in terms of Kick's law coefficient

$$\Delta C_{0^\circ} + \Delta C_{90^\circ} = \Delta C_{RI} + \Delta C_{RII} \tag{13}$$

which is equal to Eq. (8).

4.2. Estimation of C_o from material properties

If an RS-free specimen is not available, the Kick's law coefficient for the RS-free case can be estimated from material properties. FE results for C_o/E, depicted in Fig. 13, give a monotonic increase with ε_o and $1/n$. This is in accordance with the fact that the resistance to plastic deformation (*i.e.*, hardness) increases with yield strength and $1/n$ (which means a steeper increase of the actual yield stress with plastic strain). Data can be fitted to the following polynomial, which is quadratic in $1/n$ and cubic in ε_o,

$$\begin{aligned} &\frac{C_o}{E} = f_o(\varepsilon_o, n) = D_i(\varepsilon_o) n^{-i} \\ &D_i(\varepsilon_o) = F_{ij} \varepsilon_o{}^j \quad ; \quad i = 0,\ 1,\ 2: \quad j = 0,\ 1,\ 2,\ 3; \quad F_{oo} = 0. \end{aligned} \tag{14}$$

Coefficients are evaluated by minimizing the sum of squared relative errors. The boundary condition $F_{oo} = 0$ is added to account for the extreme, though fictitious case of a perfectly plastic material with zero-yield strain. Values for F_{ij}, based on the data for $\varepsilon_o = 0.001$, 0.002, 0.003, 0.005, 0.007, 0.01; $n = 2, 3, 5, 10, \infty$ (30 analyses), are given in Table 4. The fitting functions capture the change of C_o/E with material

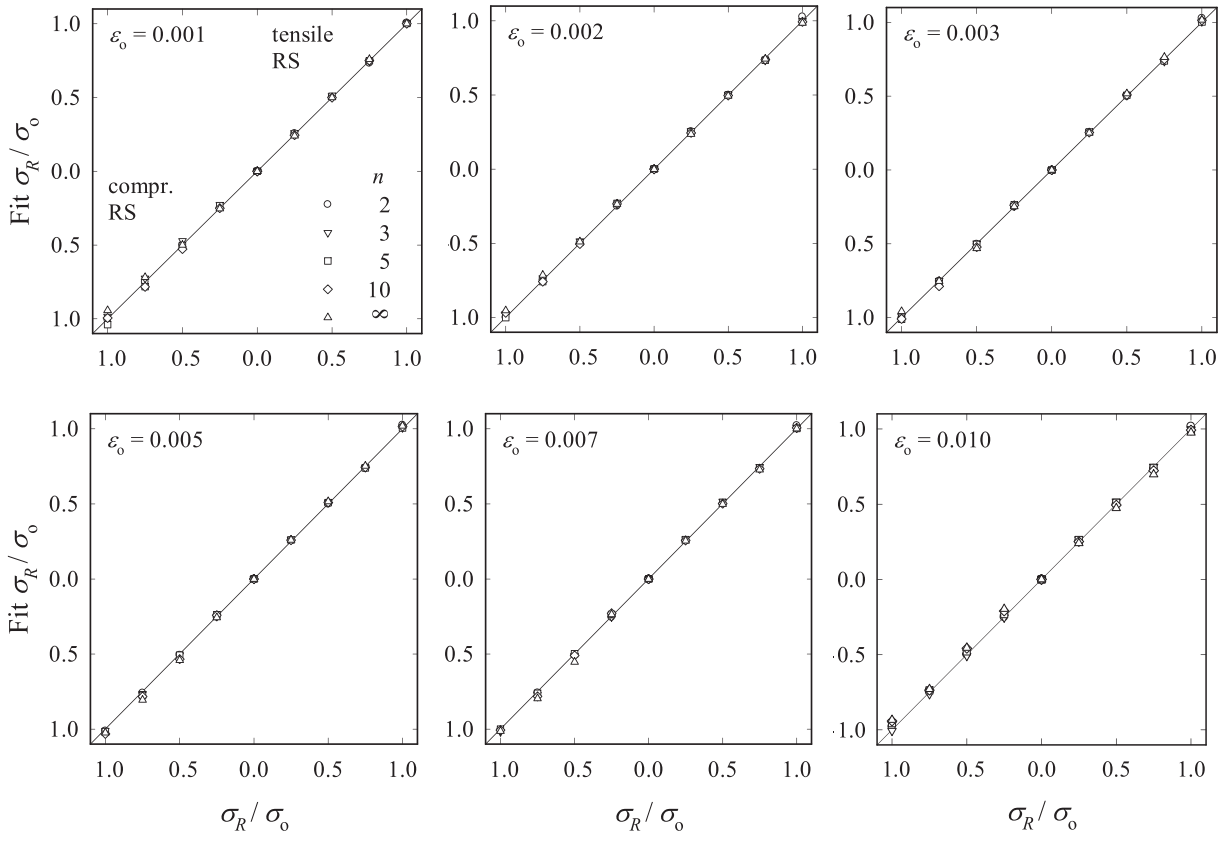

Fig. 17. Deviation of fitted σ_R/σ_o values from FE input values for σ_R/σ_o.

properties very well (Fig. 14). Fit C_o/E obtained by Eq. (14) are plotted against FE results in Fig. 15. The maximum deviation is 2.5%; the average deviation is 0.5%. However, since β and χ are quite sensitive to inaccuracies in C_o, it is generally better to obtain C_o together with $C_{0°}$ and $C_{90°}$ using the same experimental set-up.

4.3. The equibiaxial residual stress case ($\alpha = 1$)

For the equibiaxial RS case, $\chi = (C_o - C_R)/C_o$ where C_R denotes the Kick's law coefficient obtained from indentation on a specimen subject to equibiaxial RS σ_R. As we can observe in Fig. 16, χ becomes more and more sensitive to σ_R/σ_o with increasing ε_o and n – as much as C_R/C_o becomes sensitive (as discussed in Section 3). For $\varepsilon_o = 0.001$ and $n = 2$, χ lies between -0.06 ($\sigma_R = -\sigma_o$) and 0.08 ($\sigma_R = \sigma_o$), while for $\varepsilon_o = 0.01$ and $n = \infty$, χ ranges between -0.23 ($\sigma_R = -\sigma_o$) and 0.43 ($\sigma_R = \sigma_o$). Invoking the fundamental difference between the tensile and compressive RS cases, we establish separate mapping functions. Noting that for all combinations of n and ε_o, σ_R/σ_o increases monotonically with χ, we propose the following fitting function

$$\begin{aligned} &\frac{\sigma_R}{\sigma_o} = f_R^{+/-}(\chi, \varepsilon_o, n) = G_i^{+/-}(\varepsilon_o, n)\ \chi^i \quad i = 1,\ 2 \\ &G_i^{+/-}(\varepsilon_o, n) = H_{ij}^{+/-}(\varepsilon_o)\ n^{-j} \quad j = 0,\ 1,\ 2 \\ &H_{ij}^{+/-}(n) = J_{ijk}^{+/-}\ \varepsilon_o^{-k} \quad k = 0,\ 1,\ 2\,. \end{aligned} \tag{15}$$

The plus and minus superscripts denote functions for tensile and compressive RS, respectively. The fitting coefficients for $f_R^{+/-}$, listed in Table 5, are evaluated based on data for $\sigma_R/\sigma_o = \pm 0.25, \pm 0.5, \pm 0.75, \pm 1.0$; $\varepsilon_o = 0.001, 0.002, 0.003, 0.005, 0.007, 0.01$; $n = 2, 3, 5, 10, \infty$ (240 analyses). The fitting functions $f_R^{+/-}$ describe the material behavior accurately (Fig. 17).

4.4. The biaxial residual stress case ($0 \le \alpha \le 1$)

Having related β to α and χ to σ_R, we can determine biaxial RS as follows. Material properties E, σ_o and n are assumed to be known. They may be determined by indentation – *e.g.,* the spherical indentation technique by Lee et al. [28] or the dual indenter technique proposed by Chollacoop et al. [29] – or by fitting uniaxial tensile test data to Eq. (1). C_o is either obtained from Knoop indentation of an RS-free specimen, or calculated by Eq. (14) if an RS-free specimen is unavailable. Alternatively, an RS-free state can be established by cutting the specimen so that a micro-pillar, the height of which should exceed its diameter, remains [30]. From indentation on this pillar, C_o can be obtained. Though more cumbersome, this method is especially useful for thin films or coatings. Having determined $C_{0°}$ and $C_{90°}$ from two Knoop indentations, we compare them with C_o to check whether RS are tensile or compressive. If RS are sufficiently high, *i.e.,* $|\chi| \ge \chi^* = 0.01$ (see below), the stress ratio α is calculated by Eq. (6). This α value must be equal to the RS ratio σ_{RI}/σ_{RII} of two virtual equibiaxial RS cases giving C_{RI} and C_{RII} (Roman numerals are used to denote reference to the virtual equibiaxial case). The corresponding χ values, χ_I and χ_{II}, become

$$\chi_I = \frac{C_o - C_{RI}}{C_o} \quad ; \quad \chi_{II} = \frac{C_o - C_{RII}}{C_o} = 2 - \frac{C_{0°} + C_{90°}}{C_o} - \chi_I \tag{16}$$

where we further note that χ is the mean average of $\chi_I + \chi_{II}$, *i.e.,* $\chi = (\chi_I + \chi_{II})/2$. Inserting Eq. (16) into Eq. (15) and noting that χ_{II} depends on χ_I, we solve

$$\frac{\sigma_{RI}}{\sigma_{RII}} - \alpha = \frac{f_R^{+/-}(\chi_I, \varepsilon_o, n)}{f_R^{+/-}(\chi_{II}, \varepsilon_o, n)} - \alpha = 0 \tag{17}$$

for χ_I. Note that since 2nd degree polynomial functions are used for relating χ to σ_R/σ_o, we can directly solve for χ_I. σ_{R1} is then calculated by inserting χ_I into Eq. (15), and $\sigma_{R2} = \sigma_{R1}/\alpha$. The algorithm for determining RS is illustrated in Fig. 18. As above, apart from $\varepsilon_o = 0.001$, where there is some deviation, final results for σ_{R1} and σ_{R2} are in a good agreement with corresponding FE input values (Fig. 19), which shows the accuracy of the fitting functions.

Some short remark shall be given to the case of very small RS. As noted above, the definition of β is not suitable when *both* RS approach zero, *i.e.,* $C_{0°} \approx C_{90°} \approx C_o$, because β becomes increasingly sensitive to small inaccuracies in C values, especially for materials with low ε_o and high n. Nevertheless, in such a case (of very low RS) we can determine whether RS are tensile or compressive. If we assume that the stress ratio is not important – for example, when one wants to find the region of zero RS –, we can make an estimate regarding the magnitude of RS. Using $\alpha = 1$ and inserting χ into Eq. (15) delivers an RS value that is representative of the magnitude of RS. Of course, here the Knoop indenter has no advantage over other indenters.

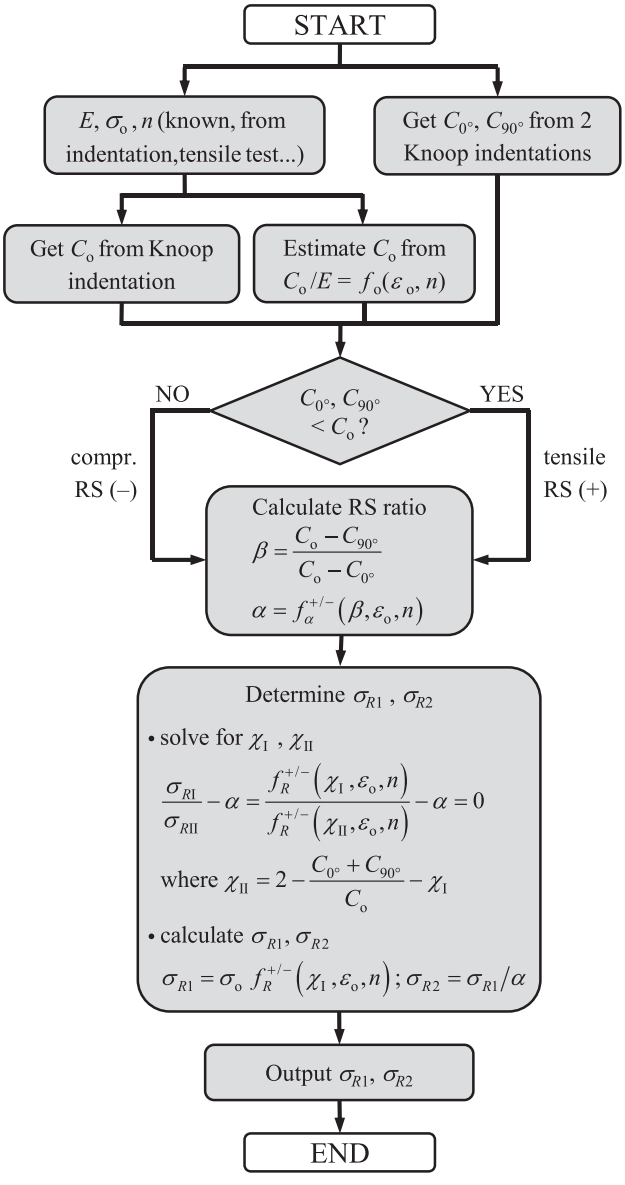

Fig. 18. Algorithm for determination of RS.

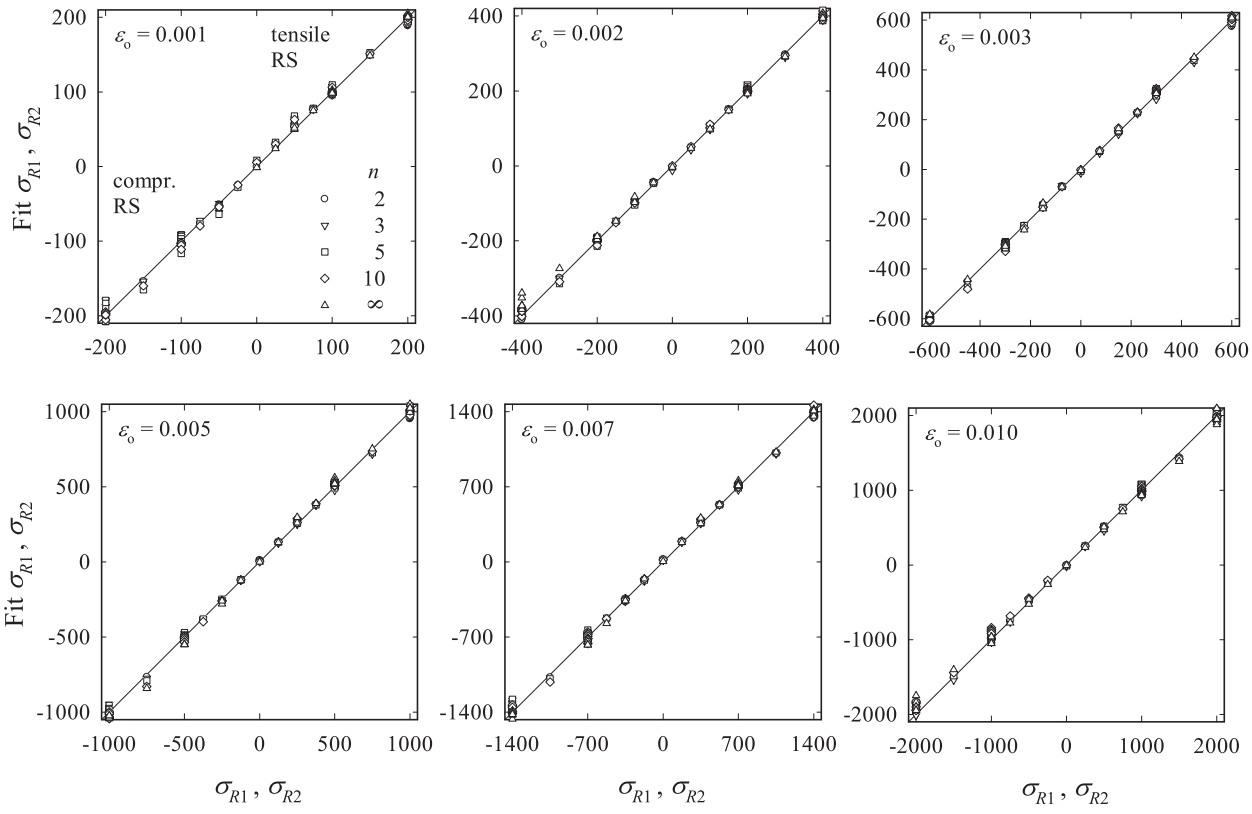

Fig. 19. Deviation of fit σ_{R1} and σ_{R2} from corresponding FE input values.

5. Experimental validation by Knoop indentation tests on bended specimens

To assess the suggested method, Knoop micro-indentation tests are performed using a custom-made instrumented micro-indentation system with a capacity of 500 kgf and a load resolution of 5 gf. The indentation depth resolution of the linear encoder is 0.05 μm. The displacement is controlled by an AC servo actuator with a maximum torque of 6.5 kgf m. Material properties of structural steel JIS SS400 and carbon steel SM45C – each annealed at 780 °C and subsequently furnace-cooled to remove RS – are obtained by indentation with WC spherical indenters (E = 537 GPa) of 1 mm diameter (indentation depth 0.2 mm, velocity 0.3 mm/min). The procedure for deriving E (based on the Oliver–Pharr method; [31,32]), σ_o and n is explained in Lee et al. [28]. Indentation load and obtained material properties are provided in Table 1; Poisson's ratio is $\nu = 0.3$. Excluding upper and lower outliers, mean average values are taken as material properties. Both materials lie more or less in the middle of the range of ε_o and n. Tensile tests reveal that the stress–strain curves of the two materials follow the Hollomon-type stress–strain relation in Eq. (1) properly.

Adopting the design of the device proposed by Lee and Kwon [18], which was similar to the set-up by Tsui *et al.* [3], we employ a cross-shaped specimen as depicted in Fig. 20. Biaxial tensile RS are induced by elastically deflecting the ends of the specimen *via* an adjustment

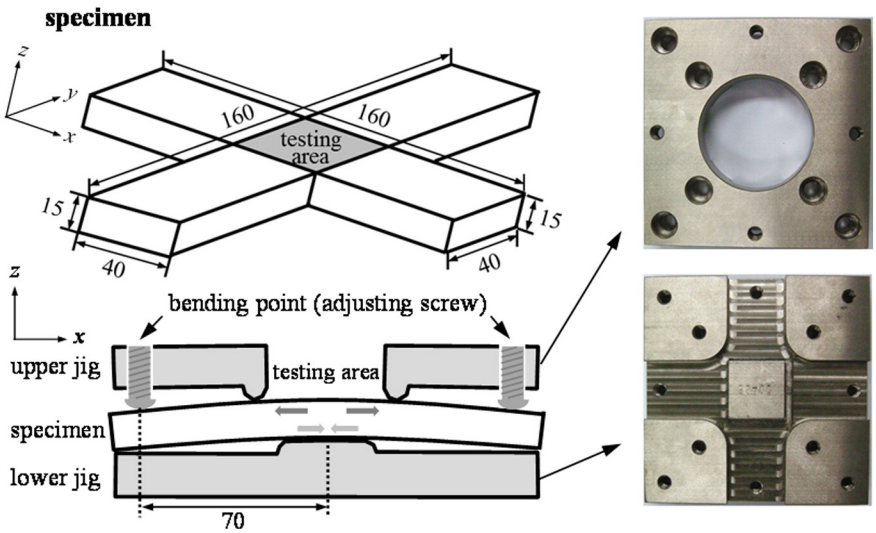

Fig. 20. Bending specimen and device for inducing non-equibi-axial RS (following [19]); all lengths in mm.

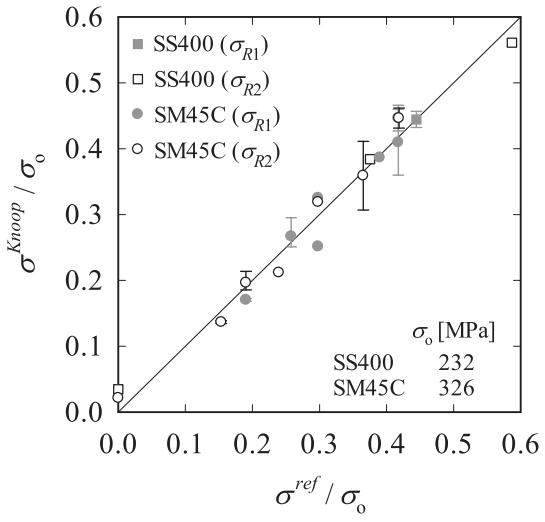

Fig. 21. RS from Knoop indentation, σ^{Knoop} *vs.* RS from strain gauge (σ^{ref}).

screw in the jig depicted in Fig. 20. Two strain gauges oriented in 1- and 2-directions are affixed to the specimen's top surface. The elastic strains are converted to reference stresses σ^{ref} using beam theory. A WC Knoop indenter penetrates the specimen surface in the center of the testing area by 50 μm with a velocity of 300 μm/min. The indentation depth (= 0.3% the specimen thickness) is chosen low enough to provide a quasi-uniform residual stress distribution and high enough that surface roughness effects on the measurement can be neglected. The load–depth curves from four subsequent indentations of the RS-free specimens can be considered coincident, which indicates that small differences in C can be sensed accurately.

From the Kick's law coefficients, we calculate the RS following the algorithm in Fig. 18 and compare them with the reference bending stresses σ^{ref} (Table 2, Fig. 21). Note that differences between indentation results for identical RS cases are at least partly because the indentation positions within the testing area are not the same. We find quite a good prediction of the RS ratio, and RS from indentation show an acceptable agreement with the bending stresses, in particular in light of the simplicity of the indentation technique.

6. Summary and concluding remarks

In this work, exploiting the asymmetry of the Knoop indenter and the resulting sensitivity of the Kick's law coefficient to its orientation with respect to the RS, we presented a method for determining non-equibiaxial RS from Knoop indentation. The approach bases exclusively on the changes of minimum and maximum C values with RS and is independent of the impression size, which may be difficult to determine accurately. Based on FE analysis results for various biaxial RS combinations and a large range of yield strains and strain hardening exponents, we could draw the following conclusions.

- FE results supported the argument that tensile and compressive RS represent fundamentally different cases; the change in C is more pronounced for tensile RS than for compressive RS.
- The RS ratio α can be determined readily from indentation variable β, independent of the magnitude of RS.
- If α is known, the non-equibiaxial RS with $C_{0°}$ and $C_{90°}$ can be converted to two virtual equibiaxial RS cases with C_{RI} and C_{RII}. The relations obtained for the equibiaxial RS case can hence be used for the case of non-equibiaxial RS.
- If RS-free specimens are unavailable, C_o can be estimated from material properties E, ε_o and n.
- The approach is in particular suitable for materials with a high yield strain and low strain hardening because these materials show a higher sensitivity of χ to σ_R/σ_o.

An algorithm was provided to illustrate the procedure for determining σ_{R1} and σ_{R2} from $C_{0°}$, $C_{90°}$ and C_o. The method was finally validated by comparison with results from Knoop indentations on elastically bended cross-shaped specimens.

Acknowledgment

This research was supported by the Basic Science Research Program through the National Research Foundation of Korea (NRF) funded by the Ministry of Science, ICT and Future Planning (No. NRF-2012 R1A2A2A 01046480).

References

[1] A. Skouras, A. Paradowsk, M.J. Peel, P.E.J. Flewitt, M.J. Pavier, Residual stress measurements in a ferritic steel/In625 superalloy dissimilar metal weldment using neutron diffraction and deep-hole drilling, Int. J. Press. Vessel. Pip. 101 (2013) 143–153.
[2] V. Hauk (Ed.), Structural and Residual Stress Analysis by Nondestructive Methods: Evaluation, Application, Assessment, Elsevier Science B.V., 1997.
[3] T.Y. Tsui, W.C. Oliver, G.M. Pharr, Influences of stress on the measurement of mechanical properties using nanoindentation: part I. Experimental studies in an aluminum alloy, J. Mater. Sci. 11 (1996) 752–759.
[4] A. Bolshakov, W.C. Oliver, G.M. Pharr, Influences of stress on the measurement of mechanical properties using nanoindentation: part II. Finite element simulations, J. Mater. Res. 11 (1996) 760–768.
[5] G. Sines and R. Carlson, Hardness measurements for determination of residual stresses, *ASTM Bulletin* 180, 35–37.
[6] S. Suresh, A.E. Giannakopoulos, A new method for estimating residual stresses by instrumented sharp indentation, Acta Mater. 46 (1998) 5755–5767.
[7] A.E. Giannakopoulos, The influence of initial elastic surface stresses on instrumented sharp indentation, J. Appl. Mech. 70 (2003) 638–643.
[8] E. Atar, C. Sarioglu, U. Demirler, E.S. Kayali, H. Cimenoglu, Residual stress estimation of ceramic thin films by X-ray diffraction and indentation techniques, Scr. Mater. 48 (2003) 1331–1336.
[9] Z.H. Xu, X. Li, Influence of equi-biaxial residual stress on unloading behaviour of nanoindentation, Acta Mater. 53 (2005) 1913–1919.
[10] S. Carlsson, P.L. Larsson, On the determination of residual stress and strain fields by sharp indentation testing. Part I: theoretical and numerical analysis, Acta Mater. 49 (2001) 2179–2191.
[11] S. Carlsson, P.L. Larsson, On the determination of residual stress and strain fields by sharp indentation testing. Part II: experimental investigation, Acta Mater. 49 (2001) 2193–2203.
[12] B. Taljat, G.M. Pharr, Measurement of residual stresses by load and depth sensing spherical indentation, Mater. Res. Soc. Symp. Proc. 594 (1999) 519–524.
[13] J.G. Swadener, B. Taljat, G.M. Pharr, Measurement of residual stress by load and depth sensing indentation with spherical indenters, J. Mater. Res. 16 (2001) 2091–2102.
[14] Z. Lu, Y. Feng, G. Peng, R. Yang, Y. Huan, T. Zhang, Estimation of surface equi-biaxial residual stress by using instrumented sharp indentation, Mater. Sci. Eng. A-Struct. 614 (2014) 264–272.
[15] M. Zhao, X. Chen, J. Yan, A.M. Karlsson, Determination of uniaxial residual stress and mechanical properties by instrumented indentation, Acta Mater. 54 (2006) 2823–2832.
[16] X. Chen, J. Yan, A.M. Karlsson, On the determination of residual stress and mechanical properties by indentation, Mater. Sci. Eng. A 416 (2006) 139–149.
[17] J. Jang, D. Son, Y. Lee, Y. Choi, D. Kwon, Assessing welding residual stress in A335 P12 steel welds before and after stress-relaxation annealing through instrumented indentation technique, Scr. Mater. 48 (2003) 743–748.
[18] Y.H. Lee, D. Kwon, Measurement of residual-stress effect by nanoindentation on elastically strained (100) W, Scr. Mater. 49 (2003) 459–465.
[19] Y.H. Lee, D. Kwon, Estimation of biaxial surface stress by instrumented indentation with sharp indenters, Acta Mater. 52 (2004) 1555–1563.
[20] J.H. Han, J.S. Lee, Y.H. Lee, M.J. Choi, G. Lee, K.H. Kim, D. Kwon, Residual stress estimation with identification of stress directionality using instrumented indentation technique, Key Eng. Mater. 345 (2007) 1125–1128.
[21] M.J. Choi, S.K. Kang, I. Kang, D. Kwon, Evaluation of nonequibiaxial residual stress using Knoop indenter, J. Mater. Res. 27 (2012) 121–125.
[22] J.H. Lee, H. Lee, H.C. Hyun, M. Kim, Numerical approaches and experimental verification of the conical indentation techniques for residual stress evaluation, J. Mater. Res. 25 (2010) 2212–2223.
[23] B.P. Groth, A.B. Mann, Identifying changes in residual stress using indentation on machined metallic surfaces, Mater. Lett. 89 (2012) 287–290.
[24] J.H. Lee, H. Lee, D.H. Kim, A numerical approach to evaluation of elastic modulus using conical indenter with finite tip radius, J. Mater. Res. 23 (2008) 2528–2537.

[25] H.C. Hyun, M. Kim, J.H. Lee, H. Lee, A dual conical indentation technique based on FEA solutions for property evaluation, Mech. Mater. 43 (2011) 313–331.
[26] Huber N. Heerens, On the effect of a general residual stress state on indentation and hardness testing, Acta Mater. 56 (2008) 6205–6213.
[27] P.L. Larsson, On the mechanical behavior at sharp indentation of materials with compressive residual stresses, Mater. Des. 32 (2011) 1427–1434.
[28] H. Lee, J.H. Lee, G.M. Pharr, A numerical approach to spherical indentation techniques for material property evaluation, J. Mech. Phys. Solids 53 (2005) 2037–2069.
[29] N. Chollacoop, M. Dao, S. Suresh, Depth-sensing instrumented indentation with dual sharp indenters, Acta Mater. 51 (2003) 3713–3729.
[30] M. Sebastiani, E. Bemporad, F. Carassiti, N. Schwarzer, Residual stress measurement at the micrometer scale: focused ion beam (FIB) milling and nanoindentation testing, Philos. Mag. 91 (2011) 1121–1136.
[31] G.M. Pharr, W.C. Oliver, F.R. Brotzen, On the generality of the relationship among contact stiffness, contact area, and elastic modulus during indentation, J. Mater. Res. 7 (1992) 813–817.
[32] W.C. Oliver, G.M. Pharr, An improved technique for determining hardness and elastic modulus using load and displacement sensing indentation experiments, J. Mater. Res. 7 (1992) 1564–1583.